Chapter 14

Turbulance

14.1 Overview

In Chap. 12, we derived the Poiseuille formula for the flow of a viscous fluid down a pipe by assuming that the flow is laminar, that is to say has a velocity parallel to the pipe. We showed how balancing the stress across a cylindrical surface led to a parabolic velocity profile and a rate of flow proportional to the fourth power of the pipe diameter, d. We also defined the Reynolds' number for pipe flow, $R \equiv \bar{v}d/\nu$, where $\bar{v}$ is the mean speed in the pipe. Now, it turns out experimentally that the flow only remains laminar up to a critical Reynolds' number that has a value that lies in the range $\sim 10^3 - 10^5$ depending upon the experimental conditions. If the pressure gradient is increased further, then the velocity field in the pipe becomes irregular both temporally and spatially, a condition we call *turbulence*.

Turbulence is common in high Reynolds' number flows. Much of our experience of fluids involves air or water for which the kinematic viscosities are $\sim 10^{-5}$ and 10^{-6}m^2 s^{-1} respectively. For a typical everyday flow with a characteristic speed of $v \sim 10$m s^{-1} and a characteristic length of $d \sim 1$m, we obtain $R = vd/\nu \sim 10^6 - 10^7$. It is therefore not surprising that we see turbulent flows all around us. Smoke in a smokestack, a cumulus cloud and the wake of a ship are three examples. In Sec. 14.2 we shall illustrate the phenomenology of the transition to turbulence as R increases using a particularly simple example, the flow of a fluid past a circular cylinder oriented perpendicular to the line of sight. We shall see how the flow pattern is dictated by the Reynolds' number and how the velocity changes from steady creeping flow to fully-developed turbulence as this parameter is increased.

But what is turbulence? Fluid dynamicists can certainly recognize it but they have a hard time defining it precisely, and an even harder time describing it quantitatively. At first glance, a quantitative description appears straightforward. Decompose the velocity field into Fourier components just like the electromagnetic field when analysing electromagnetic radiation. Then recognize that the equations of fluid dynamics are nonlinear, so there will be coupling between different modes (akin to that between the phonons discussed in Sec. 11.6). Analyze that coupling perturbatively. The resulting *weak turbulence* theory (some of which we sketch in Sec. 14.3) is useful when the turbulence is not too strong. In this approach, among other things, one averages over many realizations of a stationary turbulent flow to obtain a mean spectral energy density for the fluid's motions. Then, if this energy density extends over several octaves of wavelength, scaling arguments can be invoked to infer the shape of the energy spectrum. This furnishes the famous *Kolmogorov Law* for the turbulence spectrum. This spectrum has been verified experimentally under many different conditions. (Another theory along these lines is the *quasi-linear* theory of nonlinear plasma interactions that we shall introduce in Chap. 22.)

Most turbulent flows come under the heading of *fully-developed* or *strong turbulence* and cannot be completely described in this manner. Part of the problem is that the $(\mathbf{v}\cdot\nabla)\mathbf{v}$ term in the Navier-Stokes equation is a strong nonlinearity, not a weak coupling between linear modes. In other words, eddies persist for typically no more than one turnover timescale before they are broken up and so there are no well-defined normal modes. Another, related, problem is that it is not a good approximation to assume that the phases of the modes are random, either spatially or temporally. If we look at a snapshot of a turbulent flow, we frequently observe large, well-defined coherent structures like eddies and jets which suggest that the flow is more organized than a purely random superposition of modes, just as the light reflected from the surface of a painting differs from that emitted by a black body. Alternatively, if we monitor the time variation of some fluid variable, such as one component of the velocity at a given point in the flow we can recognize *intermittence* – the irregular starting and ceasing of turbulence. Again, this is such a marked effect that there is more than a random mode superposition at work, reminiscent of the distinction between noise and music (at least some music). Strong turbulence is therefore not just a problem in perturbation theory and alternative, semi-quantitative approaches must be devised.

In the absence of a decent quantitative theory it becomes necessary to devise intuitive, qualitative and semiquantitative approaches to the *physical* description of turbulence (Secs. 14.3 and 14.4). We emphasize the adjective physical, because our goal is to comprehend the underlying physical character of turbulence and not just to produce empirical descriptions of the consequences of turbulence. This means that the reader must be prepared to settle for order of magnitude scaling relations based on comparing the relative magnitudes of individual terms in the governing fluid dynamical equations. At first, this will seem quite unsatisfactory. However, much contemporary physics has to proceed with this methodology. It is simply too hard to discover elegant mathematical counterparts to the Kepler problem or the solution of the Schrodinger equation for the hydrogen atom.

A good example of a turbulent flow that embodies some of these principles is a turbulent boundary layer along a solid surface (Sec. 14.4). Turbulent boundary layers generally exert more shear stress on a surface than laminar boundary layers, but nevertheless usually produce less overall drag, because they are less prone to separation from the surface when subjected to an adverse pressure gradient. For this reason, turbulence is often induced artificially in boundary layers, e.g. those going over the top of an airplane wing, or those on one face of a cricket ball. In Sec. 14.4 we shall study the structure of a turbulent boundary layer and briefly discuss how its turbulence can arise through instability of a laminar boundary layer; and we shall examine some applications to balls moving through the air (golf balls, cricket balls, baseballs, ...).

One can gain additional insight into turbulence by a technique that is often useful when struggling to understand complex physical phenomena: Replace the system being studied by a highly idealized model system that is much simpler than the original one, both conceptually and mathematically, but that retains at least one central feature of the original system. Then analyze the model system completely, with the hope that the quantitative insight so gained will be useful in understanding the original problem. This approach is central to current research in quantum cosmology, where one is trying to understand how the initial conditions for the expansion of the universe were set, and to do so one works with model universes that have only a few degrees of freedom. Similarly, during the 1970's and especially the 1980's, new insights into turbulence came from studying idealized *dynamical systems* that have very small numbers of degrees of freedom, but have the same kinds of nonlinearities as produce turbulence in fluids. We shall examine several such low-dimensional dynamical systems and the insights they give in Sec. 14.5.

The most useful of those insights deal with the onset of turbulence, and the fact that it seems to have much in common with the onset of chaos in a wide variety of other dynamical systems, e.g., coupled pendula, electric circuits, and planets, asteroids, satellites and rings in the solar system. A great discovery of modern classical physics/mathematics has been that there exist organizational principles that govern the behavior of these seemingly quite different physical systems. Irregular and unpredictable dynamical behavior of dynamical systems is known collectively as *chaos*. In Sec. 14.5 we shall discuss some very simple models for the onset of chaos and shall outline the relationship of those models to the behavior of turbulent fluids.

Despite these elegant modern insights, those features of turbulence that are important in practical situations, e.g. in aeronautical or marine engineering, are still described only qualitatively and empirically. This is an indication of how far we are from a satisfactory, physical theory of turbulence.

14.2 The Transition to Turbulence - Flow Past a Cylinder

We illustrate qualitatively how a flow (and especially its transition to turbulence) depends on its Reynolds number by considering a specific problem, the flow of a uniformly moving fluid past a cylinder oriented transverse to the line of sight (Fig. 14.1). We assume that the velocity is very small compared with the speed of sound, so that the effects of compressibility can be ignored. Let the cylinder diameter be d and choose this as the characteristic length in the problem. Similarly, let the velocity far upstream be V and choose this as the characteristic velocity so that the Reynolds' number is

$$R = \frac{Vd}{\nu} \tag{14.1}$$

We assume, initially, that the flow is stationary (no turbulence) as well as incompressible. The equations governing the flow are incompressibility, $\boldsymbol{\nabla}\cdot\mathbf{v} = 0$, and the time-independent Navier-Stokes equation, Eq. (12.59) with $\partial\mathbf{v}/\partial t = 0$. These four equations (one incompressibility, three components of Navier-Stokes) can be solved for the pressure and the three components of velocity subject to the velocity vanishing on the surface of the cylinder and becoming uniform far upstream.

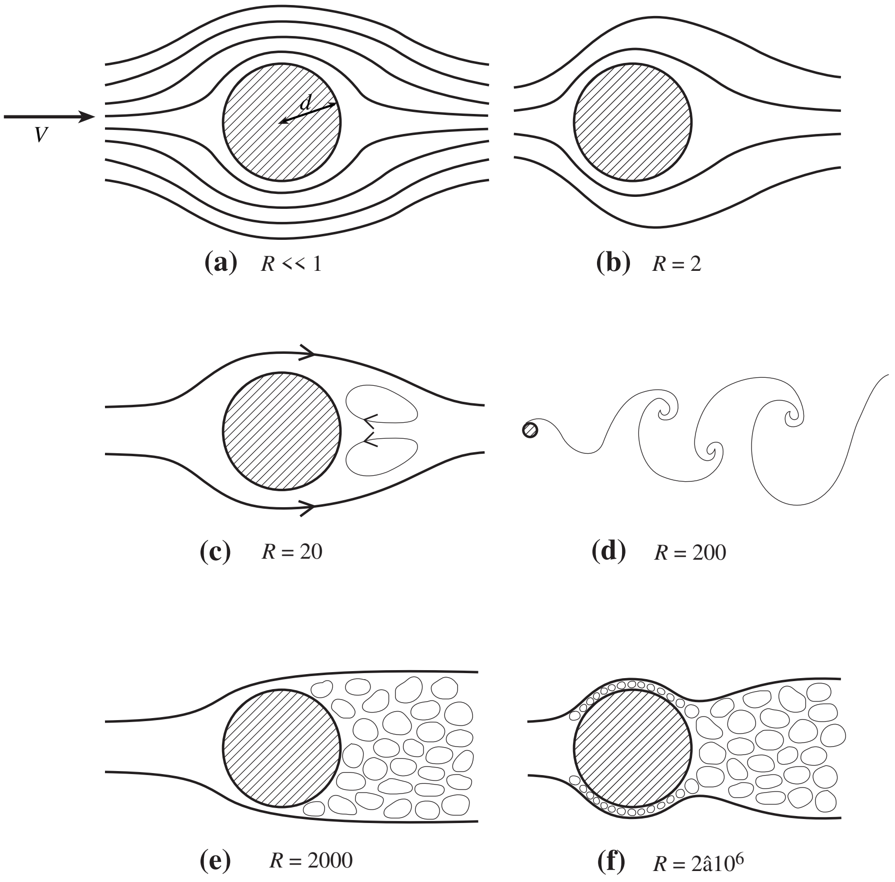

Fig. 14.1: Schematic depiction of flow past a cylinder for steadily increasing values of the Reynolds' number $R = Vd/\nu$ as labeled.

From the dimensionless parameters of the flow (the cylinder's diameter d, the fluid's incoming velocity V and its density ρ and viscosity ν) we can construct only one dimensionless number, the Reynold's number $R = Vd/\nu$. (If the flow speed were high enough that incompressibility fails, then the sound speed c_s would also be a relevant parameter and there would be a second dimensionless number, the Mach number $M = V/c_s$; Chaps. 15 and 16). With R the only dimensionless number, we are guaranteed that the solution to the flow equations can be expressed as

$$\mathbf{v}/V = \mathbf{U}(\mathbf{x}/d, R). \tag{14.2}$$

Here $\mathbf{U}$ is a dimensionless function of the dimensionless $\mathbf{x}/d$, and it can take wildly different forms depending on the value of the Reynolds' number R; cf. Fig. 14.1, which we shall discuss below.

The functional form (14.2) of $\mathbf{v}$ has important implications. If we compute the flow for specific values of the upstream velocity V, the cylinder's diameter d and the kinematic viscosity ν and then double V and d and quadruple ν so R is unchanged, then the new solution will be similar to the original solution. It can be produced from the original by rescaling the flow velocity to the new upstream velocity and the distance to the new cylinder diameter. However, if we had only doubled the kinematic viscosity, the Reynolds' number would have also doubled and we could be dealing with a qualitatively different flow.

In discussing the flow past the cylinder, a useful concept is the *stagnation pressure* in the upstream flow. This is the pressure the fluid would have, according to the Bernoulli Principle $v^2/2 + u + P/\rho + \Phi = \text{const}$, if it were brought to rest at the leading edge of the cylinder without significant action of viscosity. Ignoring the effects of compressibility and gravity (so u, ρ and Φ are constant), this stagnation pressure is $P_{\text{stag}} = P_0 + \rho V^2/2$, where P_0 is the upstream pressure. Suppose that this stagnation pressure were to act over the whole front face of the cylinder, while the pressure P_0 acted on the downstream face. The force per unit length, F, would then be $\rho V^2 d/2$. This is a first rough estimate for the drag force on the cylinder. It is conventional to define a *drag coefficient* as the ratio of the actual force per unit length to this rough estimate:

$$C_D = \frac{2F}{\rho V^2 d} \,. \tag{14.3}$$

This drag coefficient, being a dimensionless feature of the flow (14.2), can depend only on the dimensionless Reynold's number R: $C_D = C_D(R)$. Similarly for flow past a body of any other shape, C_D will be a function only of R. However, the specific functional form of $C_D(R)$ will depend on the body's shape.

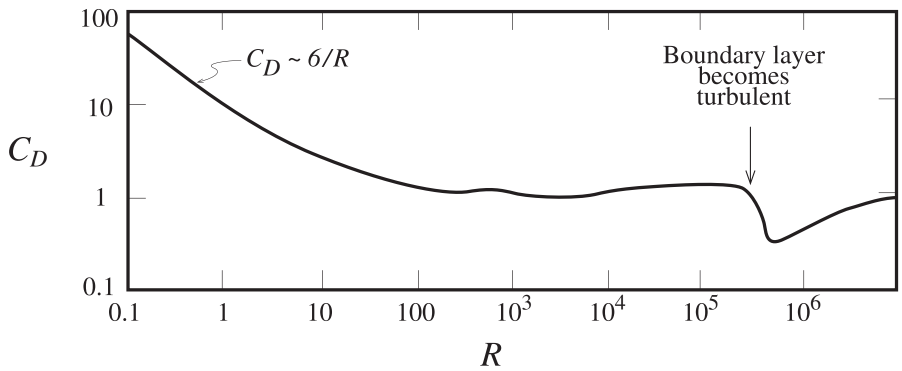

Fig. 14.2: Drag coefficient C_D for flow past a cylinder as a function of Reynolds' number $R = Vd/\nu$. This graph, adapted from Fig. 3.14 of Tritton (1977), is based on experimental measurements.

Now, turn to the details of the flow around a cylinder as described in Figs. 14.1 and 14.2. At low Reynolds' number, $R \ll 1$, there is creeping flow [Fig. 14.1(a)] just like that analyzed in detail for a spherical obstacle in Chap. 13. As you might have surmised by tackling Ex. 13.4, the details of flow past a long object such as a cylinder are subtly different from those of flow past a short one such as a sphere. This is because, for a cylinder, inertial forces become comparable with viscous and pressure forces at distances $\sim d/R$ where the flow is still significantly perturbed from uniform motion, while for short objects inertial forces become significant only at much larger radii, where the flow is little perturbed by the object's presence. Despite this, the flow streamlines around a cylinder are similar to those for a sphere and are approximately symmetric between upstream and downstream. The fluid is decelerated by viscous stresses as it moves past the cylinder along these streamlines and the pressure also decreases downstream, so that there is a net force acting on the cylinder.

The momentum removed from the flow is added to the cylinder. At $r \ll d/R$ the viscous stress dominates over the fluid's inertial stress, and the fluid momentum therefore is being transferred largely to the cyclinder, at a rate per unit area $\sim \rho V^2$, while at $r \gtrsim d/R$ the viscous and inertial stresses are comparable and balance each other, and the flow's momentum is not being transferred substantially to the cylinder. This implies that the effective cross sectional width over which the cylinder extracts the fluid momentum is $\sim d/R$, and correspondingly the net drag force per unit length is $F \sim \rho V^2 d/R$, which implies [cf. Eq. (14.3)] a drag coefficient $\sim 1/R$ at low Reynold's numbers $R \ll 1$. A more careful analysis gives $C_D \sim 6/R$, as shown experimentally in Fig. 14.2.

As the Reynolds' number is increased to ~ 1 [Fig. 14.1(b)], the effective cross section gets reduced to roughly the cylinder's geometrical width d, and correspondingly the drag coefficient decreases to $C_D \sim 1$. At this Reynold's number, $R \sim 1$, the velocity field begins to appear asymmetric from front to back.

With a further increase in R, a boundary layer of thickness $\delta \sim d/\sqrt{R}$ starts to form. The viscous force per unit length due to this boundary layer is $F \sim \rho V^2 d/\sqrt{R}$ [Eqs. (13.46)–(13.48) divided by w (with $\ell \sim d$ and $v_o = V$)]. It might therefore be thought that the drag would continue to decrease as $C_D \sim 1/\sqrt{R}$, when R decreases substantially below unity making the boundary layer thin and making the external flow start to resemble potential flow. However, this does *not* happen. Instead, at $R \sim 5$, the flow begins to separate from the back side of the cylinder and is there replaced by retrograde eddies. As described in Sec. 13.5, this separation occurs because an adverse pressure gradient $(\mathbf{v} \cdot \boldsymbol{\nabla})P > 0$ develops outside the boundary layer, near the cylinder's downstream face; and it causes the separated boundary layer to be replaced by two counter-rotating eddies [Fig. 14.1(c)]. The pressure in these eddies is of order the flow's incoming pressure P_0 and is significantly less than the stagnation pressure at the cylinder's front face, so the drag coefficient stabilizes at $C_D \sim 1$.

As the Reynold's number increases above $R \sim 5$, the size of the two eddies increases until, at $R \sim 100$, the eddies are shed dynamically, and the flow becomes non-stationary. The eddies tend to be shed alternately in time, first one and then the other, producing a pattern of alternating vortices downstream known as a *Karman vortex street* [Fig. 14.1(d)].

When $R \sim 1000$, the downstream vortices are no longer visible and the wake behind the cylinder contains a velocity field irregular on all scales [Fig. 14.1(e)]. This downstream flow has become turbulent. Finally, at $R \sim 3 \times 10^4$, the boundary layer, which has been laminar up to this point, itself becomes turbulent [Fig. 14.1(f)], reducing noticeably the drag coefficient (Fig. 14.2). We shall explore the cause of this reduction below.

An important feature of this changing flow pattern is the fact that at $R \ll 1000$ [Figs. 14.1(a)–(d)], before turbulence sets in, the flow (whether steady or dynamical) is translation symmetric; i.e., it is independent of distance z down the cylinder; i.e., it is two dimensional. This is true even of the Karman vortex street. By contrast, the turbulent velocity field at $R \gtrsim 1000$ is fully three dimensional. At these large Reynolds numbers, small, non-translation-symmetric perturbations of the translation-symmetric flow grow into vigorous, three dimensional turbulence. This is a manifestation of the fact (which we shall explore below) that two dimensional flows cannot exhibit true turbulence. True turbulence requires chaotic motions in all three dimensions.

The most important feature of this family of flows, a feature that is characteristic of most

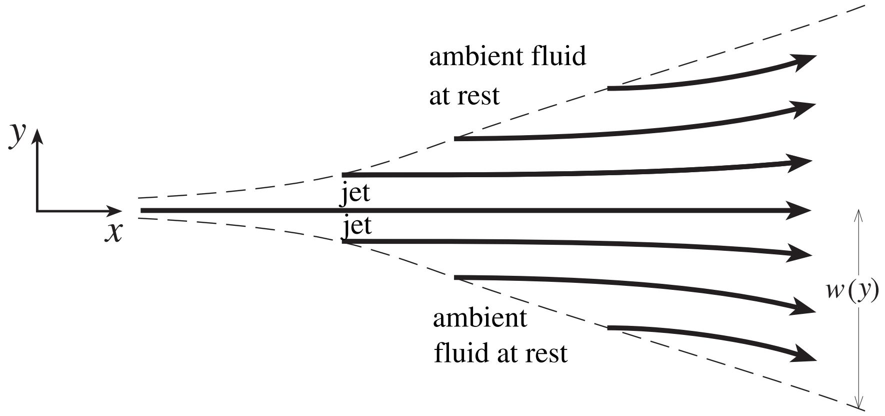

Fig. 14.3: Two dimensional laminar jet.

such families, is that there is a critical Reynolds' number for the onset of turbulence. That critical number can range from ~ 30 to $\sim 10^5$, depending on the geometry of the flow and precisely what length and speed are used to define the Reynolds' number.

****

EXERCISES

Exercise 14.1 *Example: Spreading of a laminar wake*
Consider stationary, incompressible flow around a long circular cylinder, extending perpendicular to the velocity. Let the flow far in front of the cylinder be uniform with speed V. Let the Reynolds number be small enough for the flow to remain laminar. Behind the body is a wake with width $w(x)$, at a distance x downstream from the cylinder. At the center of the wake, the flow speed is reduced to $V - \Delta v$, where Δv is called the *velocity deficit.*

(i) Use the principle of momentum conservation to derive the approximate relationship $\Delta v \propto w^{-1}$ between the velocity deficit and the width of the wake at a distance x far downstream from the cylinder. Then use the Navier-Stokes equation and invoke the principle of self-similarity as applied to the Blasius profile in Sec. 13.4 to show that $\Delta v \propto x^{-1/2}$.

(ii) How will this scaling law be modified if we replace the cylinder by a sphere?

Exercise 14.2 *Example: Spreading of Laminar Jets*
Consider a narrow, two dimensional, incompressible (i.e. subsonic) jet emerging from a two dimensional nozzle into ambient fluid of the same composition and pressure at rest. We want to understand how rapidly this jet spreads.

(i) Show that the pressure forces far downstream from the nozzle are likely to be much smaller than the viscous forces and can therefore be ignored.

(ii) Let the jet's thrust per unit length (i.e. the momentum per unit time per unit length flowing through the nozzle) be $\mathcal{F}$. Introduce cartesian coordinates x, y, with x parallel to and y perpendicular to the jet (cf. Fig. 14.3). Use the Navier-Stokes equation to make an order of magnitude estimate of the speed v_x and the width w of the jet as a function of distance x downstream in a similar manner to the previous problem.

(iii) Use these scalings to modify the analysis that we used for the laminar boundary layer in Sec. 13.4, to obtain the following approximate solution for the jet velocity profile:

$$v_x = \left(\frac{3\mathcal{F}^2}{32\rho^2\nu x}\right)^{1/3} \operatorname{sech}^2\left(\left[\frac{\mathcal{F}}{48\rho\nu^2 x^2}\right]^{1/3} y\right) .$$

****

14.3 Semi-Quantitative Analysis of Turbulence

14.3.1 Weak Turbulence

The considerations of the last section motivate us to attempt to construct a semi-quantitative, physical description of turbulence. We shall begin with an approach that is moderately reasonable for weak turbulence, but becomes much less so when the turbulence is strong: We assume that the velocity field $\mathbf{v}(\mathbf{x}, t)$ can be decomposed into a steady part $\bar{\mathbf{v}}$ plus a small, fluctuating part $\delta\mathbf{v}$, i.e. $\mathbf{v} = \bar{\mathbf{v}} + \delta\mathbf{v}$. (The bar denotes a time average.) $\bar{\mathbf{v}}(\mathbf{x})$ can be thought of as the time average of the velocity, and we shall assume it to be constant. Let us further assume, for simplicity, that the flow is incompressible. We then take the time-average of the Navier-Stokes equation (12.59) (with vanishing gravity $\mathbf{g}_e = 0$) at every point $\mathbf{x}$ in the flow to obtain

$$\rho(\bar{\mathbf{v}} \cdot \boldsymbol{\nabla})\bar{\mathbf{v}} = -\boldsymbol{\nabla} P + \nu\rho\nabla^2\bar{\mathbf{v}} - \boldsymbol{\nabla} \cdot \mathbf{T}_R, \tag{14.4}$$

where we have used $\delta\bar{\mathbf{v}} = 0$. Here

$$\mathbf{T}_R = \rho\overline{\delta\mathbf{v} \otimes \delta\mathbf{v}} \tag{14.5}$$

is known as the *Reynolds stress tensor*. It can be regarded as an additional part of the total stress tensor, analogous to the gas pressure computed in kinetic theory, $P = \frac{1}{3}\rho\overline{v^2}$, where $\mathbf{v}$ is the molecular speed (cf. Chap. 2). $\mathbf{T}_R$ will be dominated by the largest eddies present, and it can be anisotropic, especially when the largest-scale turbulent velocity fluctuations are distorted by interaction with an averaged shear flow, i.e when $\bar{\sigma}_{ij} = \frac{1}{2}(\bar{v}_{i,j} + \bar{v}_{j,i})$ is large.

If the turbulence is both stationary and homogeneous (a case we shall specialize to below when studying the "Kolmogorov spectrum"), then the Reynolds' stress tensor can be written in the form $\mathbf{T}_R = P_R\mathbf{g}$, where P_R is the Reynolds' pressure which is independent of position and $\mathbf{g}$ is the metric. In this case, the turbulence will exert no force density on the mean flow; i.e., $\boldsymbol{\nabla} \cdot \mathbf{T}_R$ will vanish in the time-averaged Navier-Stokes equation (14.4).

Notice that the Reynolds' stress tensor is the tensorial *auto-correlation* function of the velocity fluctuation field (multiplied by density ρ). It is possible to extend this "theory" of weak turbulence with the aid of a *cross-correlation* of the velocity field. The cross-correlation function involves taking the time average of products of velocity components (or other relevant physical quantities) at different points simultaneously, or at the same point at different times. (It is relatively straightforward experimentally to measure these correlation functions.) As we discuss in greater detail below (and as we also saw for one-dimensional random processes in Chap. 5 and for interfering light in Chap. 8), the Fourier transforms of these correlation functions give the spatial and temporal spectral densities of the fluctuating quantities.

14.3.2 Turbulent Diffusivity

Additional tools that are often introduced come from taking the analogy with the kinetic theory of gases one stage further and defining turbulent transport coefficients (including a turbulent viscosity) that are derived by simple analogy with the kinetic-theory transport coefficients. (For a detailed treatment of the kinetic-theory case see Chap. 2.) We recognise that momentum, heat, etc. will be transported most efficiently by the largest turbulent eddies in the flow and so we replace the particle mean free path by the size l of the largest eddies and the mean particle speed by the magnitude v_l of the fluctuations of velocity in the largest eddies. The result is a model turbulent viscosity

$$\nu_t \sim \frac{1}{3} v_l l \tag{14.6}$$

[cf. Eq. (12.68) for molecular viscosity, with $\nu = \eta/\rho$]. The Reynold's stress is then approximated as a turbulent shear stress of the standard form

$$\mathbf{T}_R \sim -2\rho\nu_t\bar{\boldsymbol{\sigma}}; \tag{14.7}$$

cf. Ex. 14.3. Here $\bar{\boldsymbol{\sigma}}$ is the rate of shear tensor from Eq. (12.40) evaluated using the mean velocity field. Note that the turbulent kinematic viscosity defined in this manner, ν_t, is a property of the turbulent flow and not an intrinsic property of the fluid; it differs from molecular viscosity in this important respect.

In the case of a gas, ν_t and the other turbulent transport coefficients can be far far larger than their kinetic-theory values. For example, air in a room subject to typical uneven heating and cooling might circulate with an average largest eddy velocity of $v_l \sim 10\text{mm s}^{-1}$ and an associated eddy size of $l \sim 10\text{m}$. (This can be estimated by observing the motion of illuminated dust particles.) The kinematic turbulent viscosity and also the diffusion coefficient associated with these motions are $\sim 10^{-2}\text{m}^2\text{s}^{-1}$, some three orders of magnitude larger than the molecular values.

Similar consideration can be used to estimate a turbulent thermal conductivity for the transport of heat and a turbulent diffusivity for the transport of one component of a fluid through the other, for example an odor crossing a room.

14.3.3 Relationship to Vorticity

Three dimensional turbulent flows contain tangled vorticity. As we discussed in Chap. 13, vortex lines move with the fluid and can be stretched by the action of neighboring vortex

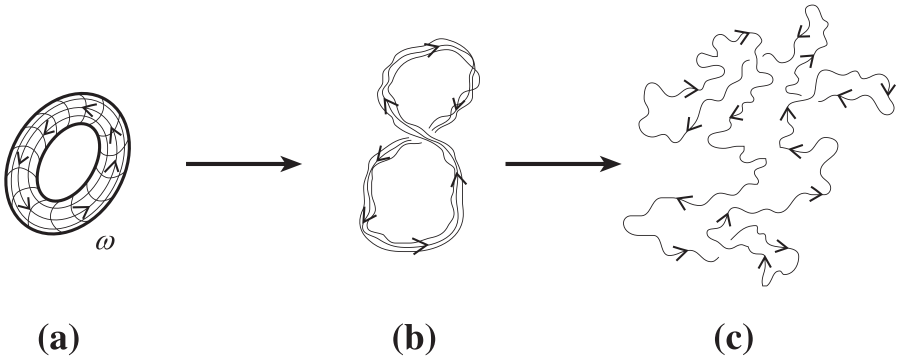

Fig. 14.4: Schematic illustration of the propagation of turbulence by the stretching of vortex lines. The tube of vortex lines in (a) gets stretched and thereby is forced into a reduced cross section by the turbulent evolution from (a) to (b) to (c). The reduced cross section means an enhanced vorticity on smaller scales.

lines. As a bundle of vortex lines is stretched and twisted (Fig. 14.4), the incompressibility of the fluid causes the bundles's cross section to decrease and correspondingly causes the magnitude of its vorticity to increase, and the lengthscale on which the vorticity changes to decrease (cf. Sec. 13.2). The continuous lengthening and twisting of the fluid therefore creates vorticity on progressively smaller length scales.

Note that, when the flow is two dimensional (i.e. translation symmetric), there is no stretching of the vortex lines and thus no inexorable driving of the turbulent energy to smaller and smaller length scales. This is one reason why true turbulence does not occur in two dimensions, only in three.

14.3.4 Kolmogorov Spectrum for Homogeneous and Isotropic Turbulence

When a fluid exhibits turbulence over a large volume that is well-removed from any solid bodies, then there will be no preferred directions and no substantial gradients in the statistically-averaged properties of the turbulent velocity field. This suggests that the turbulence will be stationary and isotropic. We shall now derive a semi-quantitative description of some of the statistical properties of such stationary, isotropic turbulence. Our derivation will be based on the following physical model:

We shall idealize the turbulent velocity field as made of a set of large eddies, each of which contains a set of smaller eddies and so on. We suppose that each eddy splits into eddies roughly half its size after a few turnover times. This can be described mathematically as nonlinear or triple velocity correlation terms producing, in the law of energy conservation, an energy transfer (a "cascade" of energy) from larger scale eddies to smaller scale eddies. Now, for large enough eddies, we can ignore the effects of genuine viscosity in the flow. However, for small enough length scales, viscous dissipation will convert the eddy bulk kinetic energy into heat. This simple model will enable us to derive a remarkably successful formula (the "Kolmogorov spectrum") for the distribution of turbulent energy over eddy size.

We must first introduce and define the turbulent energy per unit wave number and per unit mass, $U_k(k)$. Consider the Fourier transform $\delta\tilde{\mathbf{v}}(\mathbf{k})$ of the fluctuating velocity field $\delta\mathbf{v}(\mathbf{x})$:

$$\delta\mathbf{v} = \int_V \frac{d^3k}{(2\pi)^3}\delta\tilde{\mathbf{v}}e^{i\mathbf{k}\cdot\mathbf{x}} \ . \tag{14.8}$$

We perform this Fourier transform in much the same way that we take the Fourier transform of the wave function ψ in quantum mechanics: we introduce an imaginary, cubical "box" of volume V and side $V^{1/3}$ in which to compute the transform, we require that V be much larger than the volumes of the largest turbulent eddies, and we treat $\delta\mathbf{v}$ mathematically as though it vanished outside the box's walls. We then define the total energy per unit mass U in the turbulence by

$$\begin{aligned} U = \int \frac{d^3x}{V}\frac{1}{2}\overline{|\delta\mathbf{v}|^2} &= \int \frac{d^3k}{(2\pi)^3}\frac{\overline{|\delta\tilde{\mathbf{v}}|^2}}{2V} \\ &= \int_0^\infty dk\, U_k(k) \ , \end{aligned} \tag{14.9}$$

where

$$U_k(k) = \frac{\overline{|\delta\tilde{\mathbf{v}}|^2}k^2}{4\pi^2 V}. \tag{14.10}$$

Here the bars denote a time average, k is the magnitude of the wave vector $k \equiv |\mathbf{k}|$ (i.e. it is the wave number or equivalently 2π divided by the wavelength), and $U_k(k)$ is the *spectral energy per unit mass* of the turbulent velocity field $\delta\mathbf{v}$. In the second equality in Eq. (14.9), we have assumed that the turbulence is isotropic so the integrand depends only on wave number k and not on the direction of $\mathbf{k}$. Correspondingly, we have defined $U_k(k)$ as the energy per unit wave number rather than an energy per unit volume of $\mathbf{k}$-space. Therefore, $U_k(k)dk$ is the average kinetic energy per unit mass associated with modes that have k lying in the interval dk; we treat k as positive.

In Chap. 5 we introduced the concept of a "random process" and its "spectral density." The Cartesian components of the fluctuating velocity δv_x, δv_y, δv_z obviously are random processes, and it is straightforward to show that their spectral densities are related to $U_k(k)$ by

$$G_{v_x}(k) = G_{v_y}(k) = G_{v_z}(k) = \text{const} \times U_k(k), \tag{14.11}$$

where the constant is of order unity.

We shall now use our physical model of turbulence to derive an expression for $U_k(k)$. Denote by $k_{min} = 2\pi/l$ the wave number of the largest eddies, and by k_{max} that of the smallest ones (those in which viscosity dissipates the cascading, turbulent energy). Our derivation will be valid, and the result will be valid, only when $k_{max}/k_{min} \gg 1$, i.e. only when there is a large sequence of eddies from the largest to half the largest to a quarter the largest ... down to the smallest.

As a tool in computing $U_k(k)$, we introduce the root-mean-square turbulent turnover speed of the eddies with wave number k, $v(k) \equiv v$; and ignoring factors of order unity, we treat the size of these eddies as k^{-1}. Then their turnover time is $\tau(k) \sim k^{-1}/v(k) = 1/[kv(k)]$. Our model presumes that in this same time τ (to within a factor of order unity), each eddy

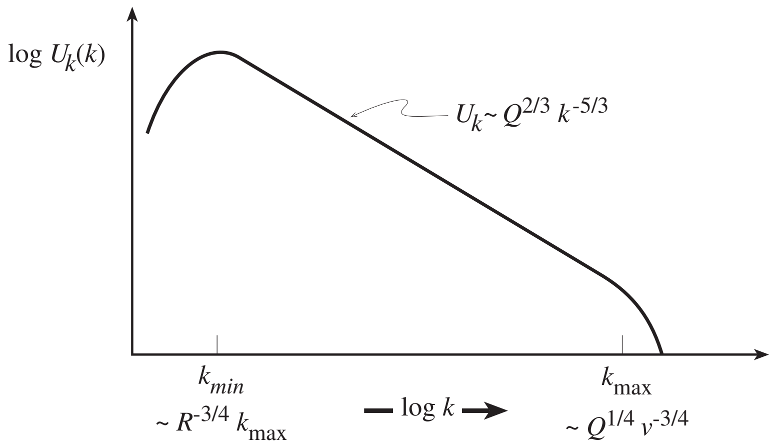

Fig. 14.5: The Kolmogorov spectral energy density for stationary, homogeneous turbulence.

of size k^{-1} splits into eddies of half this size; i.e. the turbulent energy cascades from k to $2k$. Since the energy cascade is presumed stationary (i.e. no energy is accumulating at any wave number), the energy per unit mass that cascades in a unit time from k to $2k$ must be independent of k. Denote by Q that k-independent, cascading energy per unit mass per unit time. Since the energy per unit mass in the eddies of size k^{-1} is v^2 (aside from a factor 2, which we neglect), and the cascade time is $\tau \sim 1/(kv)$, then $Q \sim v^2/\tau \sim v^3 k$. This tells us that the rms turbulent velocity is

$$v(k) \sim (Q/k)^{1/3}. \tag{14.12}$$

Our model lumps together all eddies with wave number within a range $\Delta k \sim k$ around k, and treats them all as having wave number k. The total energy per unit mass in these eddies is $U_k(k)\Delta k \sim kU_k(k)$ when expressed in terms of the sophisticated quantity $U_k(k)$, and it is $\sim v(k)^2$ when expressed in terms of our simple model. Thus, our model predicts that $U_k(k) \sim v(k)^2/k$, which by Eq. (14.12) implies

$$U_k(k) \sim Q^{2/3} k^{-5/3} \;\text{ for } k_{min} \ll k \ll k_{max}; \tag{14.13}$$

see Fig. 14.5. This is the *Kolmogorov spectrum* for the spectral energy density of stationary, isotropic, incompressible turbulence. It is valid only in the range $k_{min} \ll k \ll k_{max}$ because only in this range are the turbulent eddies continuously receiving energy from larger lengthscales and passing it on to smaller scales. At the ends of the range, the spectrum will be modified in the manner illustrated qualitatively by Fig. 14.5.

The smallest lengthscales present, k_{max}^{-1}, are determined by the fact that there viscous forces become competitive with inertial forces in the Navier-Stokes equation, and thereby convert the cascading energy into heat. Since the ratio of inertial forces to viscous forces is the Reynolds number, the smallest eddies have a Reynolds number of order unity: $R_{k_{max}} = v(k_{max})k_{max}^{-1}/\nu \sim 1$. Inserting Eq. (14.12) for $v(k)$, we obtain

$$k_{max} \sim Q^{1/4}\nu^{-3/4}. \tag{14.14}$$

The largest eddies have sizes $l \sim k_{min}^{-1}$ and turnover speeds $v_l = v(k_{min}) \sim (Q/k_{min})^{1/3}$. By combining these relations with Eq. (14.14) we see that the ratio of the largest wave numbers present in the turbulence to the smallest is

$$\frac{k_{max}}{k_{min}} \sim \left(\frac{v_l l}{\nu}\right)^{3/4} = R^{3/4}. \tag{14.15}$$

Here R is the Reynolds number for the flow's largest eddies.

Let us now take stock of our results: If we know the scale l of the largest eddies and their rms turnover speeds v_l (and, of course, the viscosity of the fluid), then from these we can compute their Reynolds number R; from that, Eq. (14.15), and $k_{min} \sim l^{-1}$, we can compute the flow's maximum and minimum wave numbers; and from $Q \sim v_l^3/l$ and Eq. (14.13) we can compute the spectral energy density in the turbulence.

We can also compute the total time required for energy to cascade from the largest eddies to the smallest: Since $\tau(k) \sim 1/(kv) \sim 1/(Q^{1/3}k^{2/3})$, each successive set of eddies feeds its energy downward in a time $2^{-2/3}$ shorter than the preceeding set. As a result, it takes roughly the same amount of time for energy to pass from the second largest eddies (size $l/2$) to the very smallest (size k_{max}^{-1}) as it takes for the second largest to extract the energy from the very largest. The total cascade occurs in a time of several l/v_l (during which time, of course, the mean flow has fed new energy into the largest eddies and they are sending it on downwards).

These results are accurate only to within factors of order unity – with one major exception: The $-5/3$ power law in the Kolmogorov spectrum is very accurate. That this ought to be so one can verify in two equivalent ways: (i) Repeat the above derivation inserting arbitrary factors of order unity at every step. These factors will influence the final multiplicative factor in the Kolmogorov spectrum, but will not influence the $-5/3$ power. (ii) Notice that the only dimensioned entitities that can influence the spectrum in the region $k_{min} \ll k \ll k_{max}$ are the energy cascade rate Q and the wave number k. Then notice that the only quantity with the dimensions of $U_k(k)$ (energy per unit mass per unit wave number) that can be constructed from Q and k is $Q^{2/3}k^{-5/3}$. Thus, aside from a multiplicative factor of order unity, this must be the form of $U_k(k)$.

Let us now review and critique the assumptions that went into our derivation of the Kolmogorov spectrum. First, we assumed that the turbulence is stationary and homogeneous. Real turbulence is neither of these, since it exhibits intermittency (Sec. 14.1) and smaller eddies tend to occupy less volume overall than larger eddies. Second, we assumed that the energy source is large-length-scale motion and that the energy transport is local in k-space from the large length scales to steadily smaller ones. In the language of a Fourier decomposition into normal modes, we assumed that nonlinear coupling between modes with wave number k causes modes with wave number of order $2k$ to grow, but does not significiantly enhance modes with wave number $100k$ or $0.01k$. Again this is not completely in accord with observations which reveal the development of *coherent structure*–large scale regions with correlated vorticity in the flow. These structures are evidence for a reversed flow of energy in k-space from small scales to large scales, and they play a major role in another feature of real turbulence, *entrainment* – the spreading of an organised motion, e.g. a jet, into the surrounding fluid (Ex. 14.6).

Despite these qualifications, the Kolmogorov law is surprisingly useful. It has been verified in many laboratory flows. It describes many naturally occuring instances of turbulence. For example, the twinkling of starlight is caused by refractive index fluctuations in the earth's atmosphere, whose power spectrum we can determine optically. The underlying turbulence spectrum turns out to be of Kolmogorov form.

****

EXERCISES

Exercise 14.3 *Example: Reynolds' Stress*

(i) Derive Eq. (14.5) for the definition of the Reynolds' stress. This equation shows how the Reynolds' stress affects the evolution of the mean velocity. However, it does not tell us how the Reynolds' stress evolves.

(ii) Show that an equation for the evolution of the Reynolds' stress involves averages of triple products of the velocity fluctuation. How do you think you might "close" this sequence of equations?

(iii) Derive an equation for the fluctuating part of the Navier-Stokes equation,

$$\frac{\partial\delta\mathbf{v}}{\partial t}+(\bar{\mathbf{v}}\cdot\boldsymbol{\nabla})\delta\mathbf{v}+(\delta\mathbf{v}\cdot\boldsymbol{\nabla})\bar{\mathbf{v}}+[(\delta\mathbf{v}\cdot\boldsymbol{\nabla})\delta\mathbf{v}-\overline{(\delta\mathbf{v}\cdot\boldsymbol{\nabla})\delta\mathbf{v}}]=-\frac{1}{\rho}\boldsymbol{\nabla}P+\nu\nabla^2(\delta\mathbf{v}).$$

From this, derive the law of evolution of turbulent energy,

$$\bar{\mathbf{v}}\cdot\boldsymbol{\nabla}(\frac{1}{2}\rho\overline{\delta v^2})+\boldsymbol{\nabla}\cdot\overline{(\frac{1}{2}\rho\delta v^2\delta\mathbf{v}+P\mathbf{v})}=-\mathbf{T}_R^{ij}\bar{v}_{i,j}+\nu\rho\overline{\delta\mathbf{v}\cdot(\nabla^2\delta\mathbf{v})}\;.$$

Interpret each term in this equation.

(iv) Now derive a similar law for the conservation of the energy of the ordered motion $\frac{1}{2}\rho\bar{\mathbf{v}}^2$. Show that the energy lost by the ordered motion is compensated by the energy gained by the turbulent energy.

Exercise 14.4 *Example: Turbulent Wake*
Consider a turbulent wake formed by high Reynolds' number flow past a cylinder, as in Ex. 14.1. Let the width a distance x downstream be $w(x)$ the flow speed far upstream be V and the velocity deficit in the mean velocity field of the wake be $\Delta\bar{v}$.

(i) Argue that the kinematic turbulent viscosity in the wake should be $\nu_t\sim\Delta\bar{v}w$. Hence, using a similar order of magnitude analysis to that given in Ex. 14.1, show that the width of the wake is $w\sim(xd)^{1/2}$, where d is the cylinder diameter, and that the velocity deficit is $\Delta v\sim V(d/x)^{1/2}$.

(ii) Repeat this exercise for a sphere.

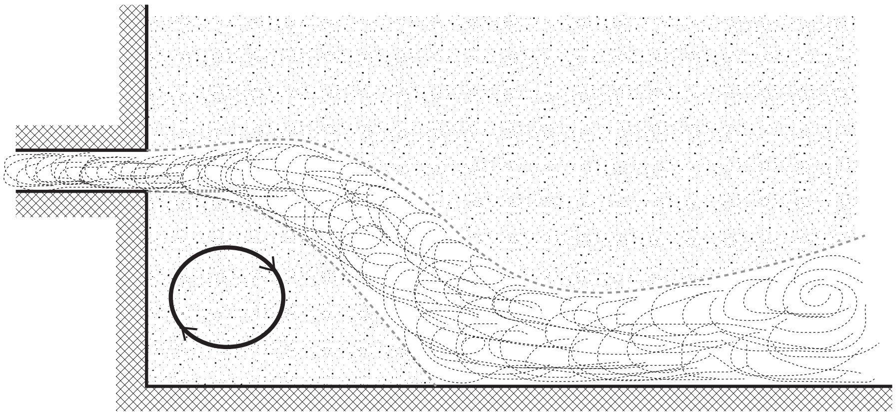

Fig. 14.6: The Coanda effect. A turbulent jet emerging from an orfice in the left wall is attracted by the solid bottom wall.

Exercise 14.5 *Problem: Turbulent Jet*
Now consider a two dimensional, turbulent jet emerging into an amient fluid at rest, and contrast it to the laminar jet analyzed in Ex. 14.2.

(i) Find how the velocity and jet width scale with distance downstream from the nozzle.

(ii) Repeat the exercise for a three dimensional jet.

Exercise 14.6 *Problem: Entrainment and the Coanda Effect*

(i) Evaluate the scaling of the rate of mass flow (discharge) $\dot{M}(x)$ along the three dimensional, turbulent jet of the previous exercise. Show that it must increase with distance from the nozzle so that mass must be entrained into the flow and become turbulent.

(ii) Entrainment is responsible for the *Coanda effect* in which a turbulent jet is attracted by a solid surface (Fig. (14.6). Can you offer a physical explanation for this effect?

(iii) Compare the entrainment rate for a turbulent jet with that for a laminar jet (Ex. 14.2). Do you expect the Coanda effect to be larger for a turbulent or a laminar jet?

****

14.4 Turbulent Boundary Layers

Much interest surrounds the projection of spheres of cork, rubber, leather and string by various parts of the human anatomy, with and without the mechanical advantage of levers of willow, ceramic and the finest Kentucky ash! As is well-known, changing the surface texture, orientation, and spin of a ball in various sports can influence the trajectory markedly, and

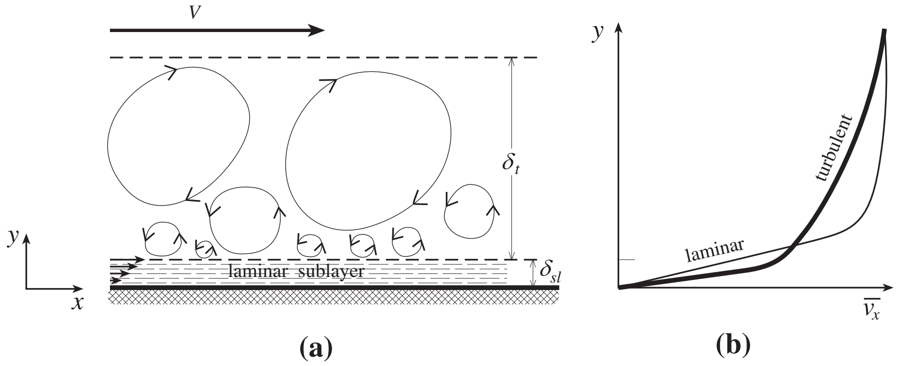

Fig. 14.7: Structure of a turbulent boundary layer.

much study has been made of ways to do this both legally and illegally. Some procedures used by professional athletes are pure superstition, but many others find physical explanations that are good examples of the behavior of boundary layers. Many sports involve the motion of balls (or indeed people) where the boundary layers can be either laminar or turbulent, and this allows opportunities for controlling the flow. With the goal of studying this, let us now consider the structure of a turbulent boundary layer—first along a straight wall, and later along a ball's surface.

14.4.1 Profile of a Turbulent Boundary Layer

In Chap. 13, we derived the Blasius profile for a laminar boundary layer and showed that its thickness a distance x downstream from the start of the boundary layer was roughly $3\delta = 3(\nu x/V)^{1/2}$, where V is the free stream speed; cf. Fig. 13.9. As we have described, when the Reynolds' number is large enough, $\sim 3 \times 10^4$ in the case of flow past a cylinder, the boundary layer itself becomes turbulent.

A turbulent boundary layer consists of a thin *laminar sublayer* of thickness δ_{ls} close to the wall and a much thicker turbulent zone of thickness δ_t. In the following paragraphs we shall use the turbulence concepts developed above to compute, in order of magnitude, the structure of the laminar sublayer and the turbulent zone, and the manner in which those structures evolve along the boundary. We denote by y distance perpendicular to the boundary, and by x distance along it in the direction of the flow.

One key to the structure of the boundary layer is the fact that, in the x component of the time-averaged Navier-Stokes equation, the stress-divergence term $T_{xy,y}$ has the potential to be so huge that no other term can compensate it. This is true in the turbulent zone, where T_{xy} is the huge Reynold's stress, and also true in the laminar sublayer, where T_{xy} is the huge viscous stress produced by a huge shear that results from the thinness of the layer. (One can check at the end of the following analysis that this dominance of $T_{xy,y}$ in the Navier-Stokes equation is indeed true for the computed boundary-layer structure.) This dominance of $T_{xy,y}$ implies that T_{xy} is (very nearly) independent of distance y from the boundary.

In the turbulent zone T_{xy} is the Reynold's stress, ρv_l^2, where v_l is the turbulent velocity of the largest eddies at a distance y from the wall; and therefore constancy of T_{xy} implies constancy of v_l. The largest eddies at y will have a size of order the distance y from the wall, and correspondingly, the turbulent viscosity will be $\nu_t \sim v_l y/3$. Equating the expression ρv_l^2 for the Reynold's stress to the alternative expression $2\rho\nu_t \bar{v}_{,y}$ (where $\bar{v}$ is the mean flow speed at y and $\bar{v}_{,y}$ is the shear), and using the above expression for the turbulent viscosity, we discover that in the turbulent zone the mean flow speed varies logarithmically with distance from the wall: $\bar{v} \sim v_l \ln y + \text{constant}$. Since the turbulence is created at the inner edge of the turbulent zone, $y \sim \delta_{sl}$, by interaction of the mean flow with the laminar sublayer, the largest turbulent eddies there must have their turnover speeds v_l equal to the mean-flow speed there: $\bar{v} \sim v_l$ at $y \sim \delta_{sl}$. This tells us the normalization of the logarithmically varying mean flow speed:

$$\bar{v} \sim v_l[1 + \ln(y/\delta_{sl})] \quad \text{at } y \gtrsim \delta_{sl}. \tag{14.16}$$

Turn, next to the structure of the laminar sublayer. There the constant shear stress is viscous, $T_{xy} = \rho\nu\bar{v}_{,y}$; and stress-balance at the interface between the laminar sublayer and the turbulent zone requires that this viscous stress be equal to the turbulent zone's ρv_l^2. This equality implies a linear profile for the mean flow velocity in the laminar sublayer, $\bar{v} = (v_l^2/\nu)y$. The thickness of the sublayer is then fixed by continuity of $\bar{v}$ at its outer edge, $(v_l^2/\nu)\delta_l = v_l$. Combining these last two relations, we obtain the following profile and sublayer thickness:

$$\bar{v} \sim v_l \left(\frac{y}{\delta_{sl}}\right) \quad \text{at } y \lesssim \delta_{sl} \sim \nu/v_l. \tag{14.17}$$

Having deduced the internal structure of the boundary layer, we turn to the issue of what determines the turbulent velocity v_l of the largest eddies. This v_l is fixed by matching the turbulent zone to the free-streaming region outside it. The free-stream velocity V must be equal to the mean flow velocity $\bar{v}$ [Eq. (14.16)] at the outer edge of the turbulent zone. The logarithmic term will dominate, so $V = v_l \ln(\delta_t/\delta_{sl})$. Introducing an overall Reynold's number for the boundary layer,

$$R_\delta \equiv V\delta_t/\nu, \tag{14.18}$$

and noting that turbulence requires a huge value of this R_δ, we can reexpress V as $V \sim v_l \ln R_\delta$. This should actually be regarded as an equation for the turbulent velocity of the largest scale eddies in terms of the free-stream velocity:

$$v_l \sim \frac{V}{\ln R_\delta}. \tag{14.19}$$

If the thickness δ_t of the entire boundary layer and the free-stream velocity V are given, then Eq. (14.18) determines the boundary layer's Reynolds' number, Eq. (14.19) then determines the turbulent velocity, and Eqs. (14.17) and (14.16) determine the layer's internal structure.

Turn, finally, to the issue of how the boundary layer thickness δ_t evolves with distance x_1 down the wall (and correspondingly, how all the rest of the boundary layer's structure, which is fixed by δ_t, evolves). At the turbulent zone's outer edge, the largest turbulent eddies move with speed v_l into the free-streaming fluid, entraining that fluid into themselves (cf. Ex. 14.6 on entrainment and the Coanda effect). Correspondingly, the thickness grows at a rate

$$\frac{d\delta_t}{dx} = \frac{v_l}{V} = \frac{1}{\ln R_\delta} \,. \tag{14.20}$$

Since R_δ depends only extremely weakly on δ_t, the turbulent boundary layer expands essentially linearly with distance x, by contrast with a laminar boundary layer's $\delta \propto x^{1/2}$.

One can easily verify that, not only does the turbulent boundary layer expand more rapidly than the corresponding laminar boundary layer would, if it were stable, but the turbulent layer is also thicker at all locations down the wall. Physically, this can be traced to the fact that the turbulent boundary layer involves a three dimensional velocity field, whereas the corresponding laminar layer would involve only a two dimensional field. The enhanced thickness contributes to an enhanced ability to withstand an adverse pressure gradient and to cling to the surface without separation (cf. Fig. 14.6 and Ex. 14.6).

However, there is a price to be paid for this benefit. Since the velocity gradient is increased close to the surface, the actual surface shear stress exerted by the turbulent layer, through its laminar sub-layer, is significantly larger than in the corresponding laminar boundary layer. As a result, if the layer were to remain laminar, that portion that would adhere to the surface would produce less viscous drag than the corresponding portion of the turbulent layer. This does *not* mean, however, that the onset of turbulence causes an increase in net drag. On the contrary, the drag goes down; cf. Fig. 14.2. The reason is that in the separated, laminar boundary layer the dominant source of drag is not viscosity but rather a pressure differential between the front face of the cylinder, where the layer adheres, and the back face where the reverse eddies circulate. The pressure is much lower in the back-face eddies than in the front-face boundary layer, and that pressure differential gives rise to a significant drag, which gets reduced when the layer goes turbulent and adheres to the back face. Therefore, if one's goal is to reduce the overall drag and the laminar flow is prone to separation, a nonseparating (or delayed-separation) turbulent layer is to be prefered over the laminar layer. Similarly (and for essentially the same reason), for an airplane wing, if one's goal is to maintain a large lift, then a nonseparating (or delayed-separation) turbulent layer is to be prefered over a separating, laminar one.

For this reason, steps are often taken in engineering flows to ensure that boundary layers become and remain turbulent. A crude but effective example is provided by the vortex generators that are installed on the upper surfaces of some airfoils. These are small obstacles on the wing which penetrate through a laminar boundary layer into the free flow. By changing the pressure, they force air into the boundary layer and initiate three dimensional vortical motion in the boundary layer forcing it to become partially turbulent. This allows airplanes to climb more steeply without stalling due to boundary-layer separation, and it helps. reduce aerodynamical drag.

14.4.2 Instability of a Laminar Boundary Layer

Much work has been done on the linear stability of laminar boundary layers. The principles behind these calculations should now be familiar, although the technical details are formidable. In the simplest case an equilibrium flow like the Blasius profile is established and the equations governing the time evolution of small perturbations are written down.

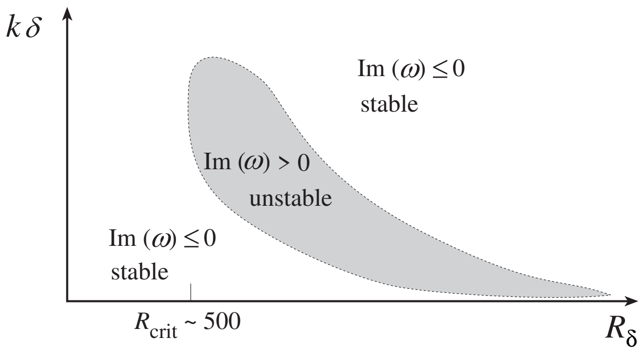

Fig. 14.8: Location of unstable wave modes in a laminar boundary layer. k is the wave number and $R_\delta = V\delta/\nu$ is the boundary layer Reynolds number.

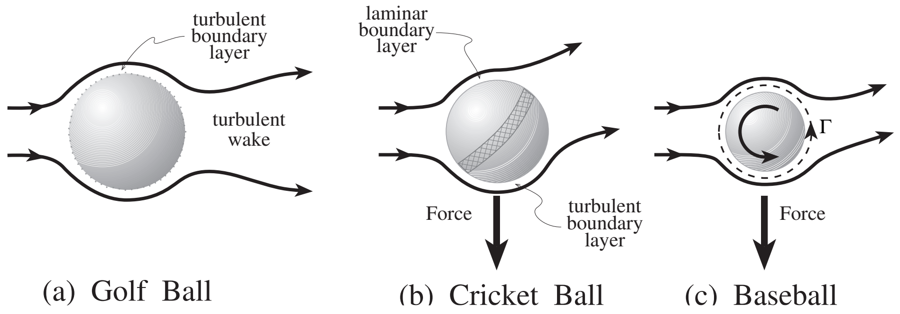

Fig. 14.9: Boundary layers around golf balls, cricket balls, and baseballs.

Spatial and temporal evolution of individual Fourier components is assumed to vary as $\exp i(\mathbf{k}\cdot\mathbf{x} - \omega t)$, and we seek modes that have zero velocity perturbation on the surface and which decay to zero in the free stream. We ask whether there are unstable modes, i.e., modes with real $\mathbf{k}$ for which the imaginary part of ω is positive so they grow exponentially in time. The results can generally be expressed in the form of a diagram like Fig. 14.8.

It is found that there is generally a critical Reynolds' number at which one mode becomes unstable. At higher values of the Reynolds' number a range of k-vectors are unstable. One interesting result of these calculations is that there has to be a point of inflection in the velocity profile (a point where d^2v_x/dy^2 changes sign) for the boundary layer to become unstable in the absence of viscous forces; cf. Ex. 14.8.

Although, in the absence of an inflection, an inviscid flow $v_x(y)$ is stable, for some such profiles viscosity can trigger instability. Physically, this is because viscosity can tap the relative kinetic energies of adjacent flow lines. Viscous-triggered instabilities of this sort are sometimes called "secular instabilities" by contrast with the "dynamical instabilities" that arise in the absence of viscosity. Secular instabilities are quite common in fluid mechanics.

14.4.3 The flight of a ball.

Having developed some insights into boundary layers and their stabilities, we now apply those insights to the balls used in various sports.

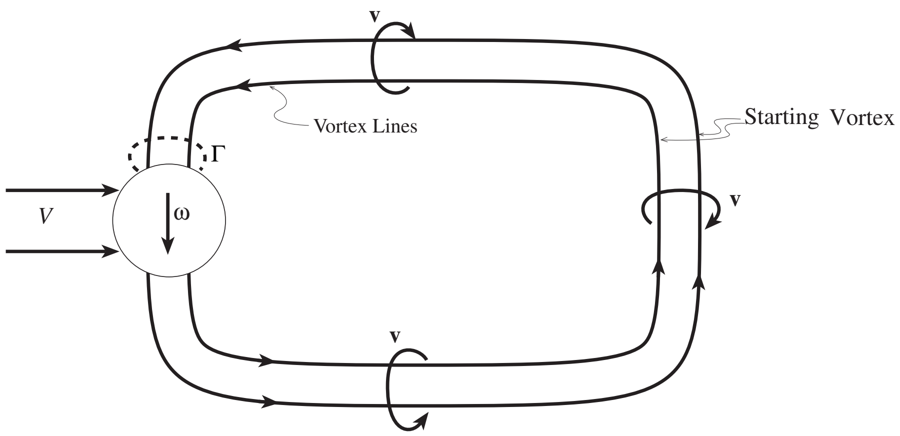

Fig. 14.10: Vortex lines passing through a spinning ball. The starting vortex is created and shed when the ball is thrown, and is carried downstream by the flow as seen in the ball's frame of reference. The vortex lines connecting this starting vortex to the ball lengthen as the flow continues.

The simplest application is to the dimples on a golf ball [Fig. 14.9(a)]. The dimples provide finite-amplitude disturbances in the flow which can initiate the formation of growing wave modes and turbulence in the boundary layer. The adherence of the boundary layer to the ball is improved and separation occurs further behind the ball leading to a lower drag coefficient and a greater range; see Figs. 14.2 and 14.9(a).

A variant on this mechanism is found in the game of cricket, which is played with a ball whose surface is polished leather with a single equatorial seam of rough stitching. When the ball is "bowled" with the seam inclined to the direction of motion, there is a laminar boundary layer on the smooth side and a turbulent boundary layer on the side with the rough seam [Fig. 14.9(b)]. These two boundary layers separate at different points behind the flow leading to a net deflection of the air. The ball can therefore swerve towards the side with the leading seam. (The effect is strongest when the ball is new and still shiny and on days when the humidity is high so the thread in the seam swells and is more efficient at making turbulence.)

This mechanism is different from that used to throw a slider or curveball in baseball, in which the pitcher causes the ball to spin about an axis roughly perpendicular to the direction of motion. In the slider the axis is vertical; for a curveball it is inclined at about 45° to the vertical. The spin of the ball creates circulation like that around an airfoil, and there is a net sideways force in the direction of the baseball's rotational velocity on its leading hemisphere, i.e. as seen by the hitter. The effect is actually quite complex and is only properly described with reference to experimental data. The major effect is that separation is delayed on the side of the ball where the rotational velocity is in the same direction as the airflow and happens sooner on the opposite side. There is a net circulation Γ; see Fig. 14.9(c). The reader may be curious as to how this circulation can be established in view of Kelvin's theorem, Eq. (13.15), which tells us that if we use a circuit that is so far from the ball and its wake that viscous forces cannot cause the vorticity to diffuse to it, then the circulation must be zero. What actually happens is that when the flow is initiated, starting vortices are shed by the ball and are then convected downstream, leaving behind the net circulation Γ that passes through the ball [Fig. 14.10]. The effect is very much larger in two dimensions with a rotating cylinder than in three dimensions because the magnitude of the shed vorticity is much larger. It goes by the name of *Magnus effect* in two dimensions and *Robins effect* in three. It is also important in understanding the lift in airfoils.

In table tennis, a drive is often hit with *topspin* so that the ball rotates about a horizontal axis perpendicular to the direction of motion. In this case, the net force is downwards and the ball falls faster toward the ground, the effect being largest after it has somewhat decelerated. This allows a ball to be hit hard over the net and bounce before passing the end of table, increasing the margin for errors in the direction of the hit.

Those wishing to improve their curveball or cure a bad slice are referred to the monographs by Adair (1990) and by Lighthill (1986).

****

EXERCISES

Exercise 14.7 *Problem: Effect of drag*
A well hit golf drive travels about 300 yards. A fast bowler or fastball pitcher throws a ball at over 90 m.p.h. A table tennis player can hit a forehand return at about 30 m.p.h. The masses and sizes of each of these three types of balls are $m_g \sim 46\text{g}, d_g \sim 43\text{mm}, m_c \sim 160\text{g}, d_c \sim 70\text{mm}, m_b \sim 140\text{g}, d_b \sim 75\text{mm}, m_{tt} \sim 2.5\text{g}, d_{tt} \sim 38\text{mm}$.

(i) For golf, cricket (or baseball) and table tennis, estimate the Reynolds' number of the flow and infer the drag coefficient, C_D. (The variation of C_D with R can be assumed to be similar to that in flow past a cylinder.

(ii) Hence estimate the importance of aerodynamic drag in determining the range of a ball in each of these three cases.

Exercise 14.8 *Problem: Tollmein-Schlicting Waves*
Consider an inviscid ($\nu = 0$), incompressible flow near a plane wall where a boundary layer is established. Introduce coordinates x parallel to the wall and y perpendicular to the wall. Let the components of the equilibrium velocity be $\{v_x(y), v_y(y), 0\}$.

(i) Show that a small perturbation in the velocity, $\delta v_y \propto \exp ik(x - ct)$, with k real and frequency ck possibly complex, satisfies the differential equation

$$\frac{d^2\delta v_y}{dy^2} = \left[\frac{1}{(v_x - c)}\frac{d^2 v_x}{dy^2} + k^2\right]\delta v_y \ .$$

Hence argue that a sufficient condition for unstable wave modes ($\text{Im}(c) > 0$), is that the velocity field possess a point of inflexion. (The boundary layer can also be unstable in the absence of a point of inflection, but viscosity must be present to trigger the instability.)

****

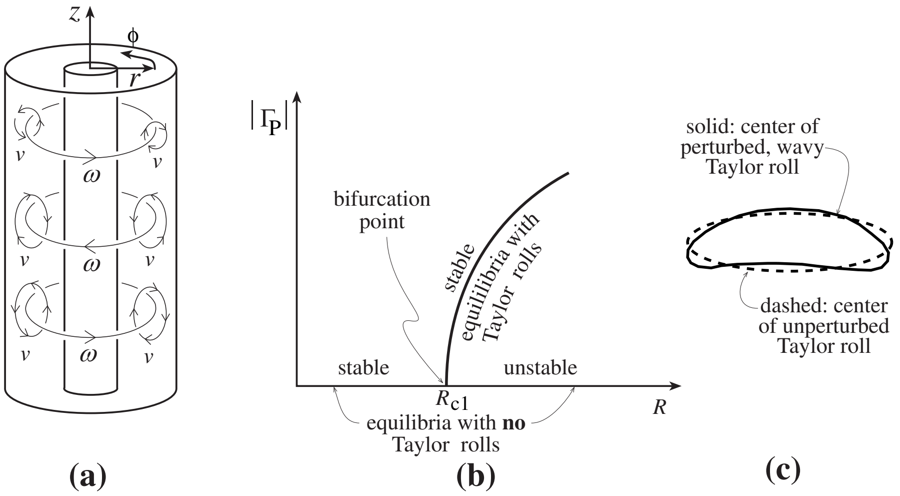

Fig. 14.11: Bifurcation in Couette flow. (a) Equilibrium flow with Taylor rolls. (b)Bifurcation diagram in which the amplitude of the poloidal circulation $|\Gamma_{\rm P}|$ in a Taylor roll is plotted against the Reynolds' number R. At low R ($R < R_{c1}$) the only equilibrium flow configuration is smooth, azimuthal flow. At larger R ($R_{c1} < R < R_{c2}$) there are two equilibria, one with Taylor rolls and stable, the other the smooth, azimuthal flow, which has become unstable. (c) Shape of a Taylor role at $R_{c1} < R < R_{c2}$ (dashed ellipse) and at higher R, $R_{c2} < R < R_{c3}$ (wavy curve).

14.5 The Route to Turbulence: Onset of Chaos

14.5.1 Couette Flow

Let us examine qualitatively how a viscous flow becomes turbulent. A good example is Couette flow between two long, concentric, relatively rotating cylinders as introduced in Chap. 13 and depicted in Fig. 14.11(a). The Rayleigh stability criterion (flow unstable if and only if angular momentum per unit mass decreases outward) was derived in Chap. 13 ignoring viscous stress. Now suppose we have a flow that is stable according to the Rayleigh criterion. Suppose, further, that the fluid is a liquid and we steadily decrease its viscosity by heating it, so that the Reynolds' number steadily increases. At low R, the equilibrium flow is stationary and azimuthal [strictly in the ϕ direction in Fig. 14.11(a)]. However, at some critical Reynolds' number R_{c1}, the flow becomes unstable to the growth of small perturbations, and these perturbations drive a transition to a new, stationary equilibrium that involves poloidal circulation (quasi-circular motions in the r and z directions, called *Taylor rolls*); see Fig. 14.11(a).

What has happened is that an equilibrium with a high degree of symmetry has become unstable and a new, lower-symmetry, stable equilibrium has taken over. Translational invariance in the direction of the cylinder axis has been lost from the flow, despite the fact that the boundary conditions remain translationally symmetric. This change of equilibrium mode is another example of a bifurcation like that discussed when we treated the buckling of beams and playing cards (Chaps. 10 and 11).

As R is increased further, this process repeats: At a second critical Reynold's number R_{c2} there is a second bifurcation of equilibria in which the azimuthally smooth Taylor rolls

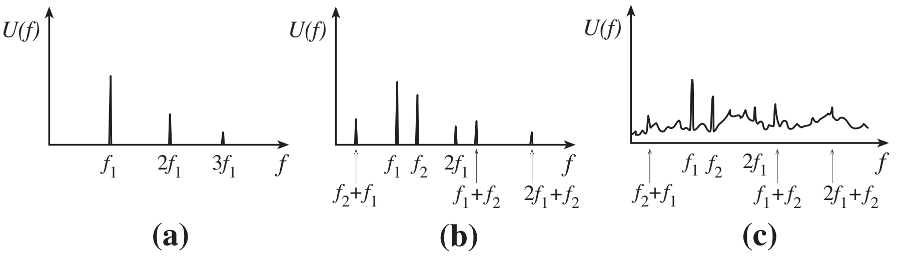

Fig. 14.12: The energy spectrum of velocity fluctuations in rotating Couette flow (schematic). (a) For a moderate Reynolds' number, $R_{c2} < R < R_{c3}$, at which the stable equilibrium flow is that with the wavy Taylor rolls of Fig. 14.11(c). (b) For a higher Reynolds' number, $R_{c3} < R < R_{c4}$, at which the stable flow has wavy Taylor rolls with two incomensurate fundamental frequencies present. (c) For a still higher Reynolds' number, $R > R_{c4}$, at which turbulence has set in.

become unstable and are replaced by new, azimuthally wavy Taylor rolls; see Fig. 14.11(c). Again, an equilibrium with higher symmetry (rotation invariance) has been replaced, at a bifurcation point, by one of lower symmetry (no rotation invariance). There is a fundamental frequency f_1 associated with the wavy Taylor rolls' motion as they circulate around the central cylinder. Since the waves are nonlinearly large, harmonics of this fundamental are also seen when one Fourier decomposes the velocity field; cf. Fig. 14.12(a). When R is increased still further to some third critical value R_{c3}, there is yet another bifurcation. The Taylor rolls now develop a second set of waves, superimposed on the first, with a corresponding new fundamental frequency f_2 that is incommensurate with f_1. In the energy spectrum one now sees various harmonics of f_1 and of f_2, as well as sums and differences of these two fundamentals; cf. Fig. 14.12(b).

It is exceedingly difficult to construct experimental apparatus that is clean enough, and free enough from the effects of finite lengths of the cylinders, to reveal what happens next as one turns up the Reynolds' number. However, despite the absence of clean experiments, it seemed obvious before the 1970's what would happen: The sequence of bifurcations would continue, with ever decreasing intervals of Reynolds' number ΔR between them, producing after awhile such a complex maze of frequencies, harmonics, sums, and differences, as to be interpreted as turbulence. Indeed, one finds the onset of turbulence described in just this manner in the classic 1959 fluid mechanics textbook of Landau and Lifshitz.

The 1970's and 1980's brought a major breakthrough in our understanding of the onset of turbulence. This breakthrough came from studies of model dynamical systems with only a few degrees of freedom, in which nonlinear effects play similar roles to the nonlinearities of the Navier-Stokes equation. These studies revealed only a handful of routes to chaos, and none were of the Landau-Lifshitz type. However, one of these routes starts out in the same manner as does rotating Couette flow: As a control parameter (Reynolds number for Couette flow) is gradually increased, first oscillations with one fundamental frequency f_1 and its harmonics turn on; then a second frequency f_2 and its harmonics turn on, along with sums and differences of f_1 and f_2; and then, suddenly, chaos sets in. Moreover, the chaos is clearly not being produced by a complicated superposition of other, new frequencies; it is fundamentally different from that. The best Couette-flow experiments of the 1980's and later appear to confirm that the onset of turbulence goes by this route; see Fig. 14.12(c).

14.5.2 Feigenbaum Sequence

The very simplest of systems in which one can study the several possible routes to chaos are one-dimensional mathematical maps. A lovely example is the "Feigenbaum sequence," explored by Mitchell Feigenbaum in the 1970's.

The Feigenbaum sequence is a sequence $\{x_1, x_2, x_3, \ldots\}$ of values of a real variable x, given by the rule (sometimes called the *logistic equation*)

$$x_{n+1} = 4ax_n(1 - x_n). \tag{14.21}$$

Here a is a fixed "control" parameter. It is easy to compute Feigenbaum sequences $\{x_n\}$ for different values of a on a pocket calculator or computer (Ex. 14.9). What is found is that there are critical parameters $a_1, a_2, \ldots$ at which the character of the sequence changes sharply. For $a < a_1$, the sequence asymptotes to a stable fixed point. For $a_1 < a < a_2$, the sequence asymptotes to stable, periodic oscillations between two fixed points. If we increase the parameter further, so that $a_2 < a < a_3$, the sequence becomes a periodic oscillation between four fixed points. The period of the oscillation has doubled. This *period doubling* (NOT frequency doubling) happens again: When $a_3 < a < a_4$, x asymptotes to regular motion between eight fixed points. Period doubling increases with shorter and shorter intervals of a until at some value a_∞, the period becomes infinite and the sequence does not repeat. Chaos has set in.

This period doubling is a second route to chaos, very different in character from the "one-frequency, two-frequencies, chaos" route that one meets in Couette flow. Remarkably, fluid dynamical turbulence can set in by this second route, as well as by the first. It does so in certain very clean experiments on convection in liquid helium. We shall return to this below, and then again in Chap. 17.

How can so starkly simple and discrete a thing as a one-dimensional map bear any relationship at all to the continuous solutions of the fluid dynamical differential equations? The answer is quite remarkable:

Consider a steady flow in which one parameter a (e.g. the Reynolds' number) can be adjusted. Now, as we change a and approach turbulence, the flow may develop a periodic oscillation with a single frequency f_1. We could measure this by inserting some probe at a fixed point in the flow to measure a fluid variable y, e.g. one component of the velocity. We can detect the periodicity either by inspecting the readout $y(t)$ or its Fourier transform $\tilde{y}$. However, there is another way, that may be familiar from classical mechanics. This is to regard $\{y, \dot{y}\}$ as the two coordinates of a two dimensional phase space. (Of course the dimensionality of the phase space could be arbitrarily large, but let us keep matters as simple as possible.) For a single periodic oscillation, the system will follow a closed path in this phase space [Fig. 14.13(a)]. As we increase a further, a period doubling may occur and the trajectory in phase space may look like Fig. 14.13(b). Now, as we are primarily interested in the development of the oscillations, we need only keep one number for every fundamental period $P_1 = 1/f_1$. Let us do this by taking a section through phase space and introducing a coordinate x on this section as shown in Fig. 14.13. The n'th time the trajectory crosses

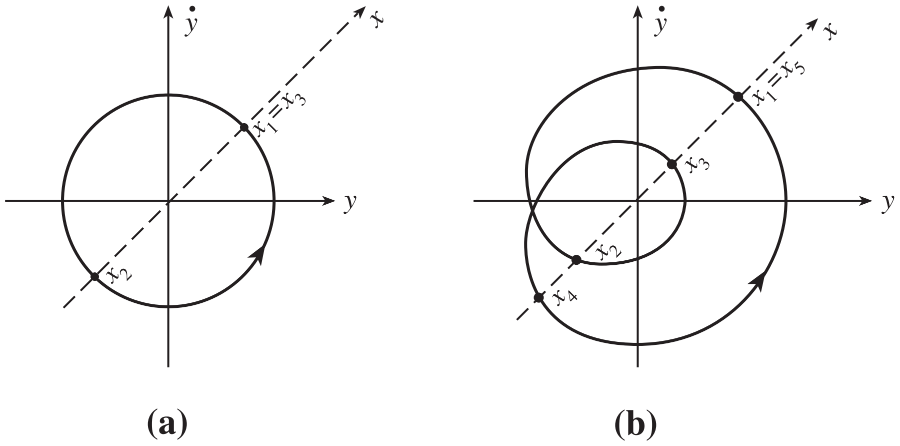

Fig. 14.13: a) Representation of a single periodic oscillation as motion in phase space. b) Motion in phase space after period doubling. The behavior of the system may be also be described by using the coordinate x of the Poincaré map.

through this section, its crossing point is x_n, and the mapping from x_n to x_{n+1} can be taken as a representative characterization of the flow. When only the frequency f_1 is present, the map will read $x_{n+2} = x_n$ [Fig. 14.13(a)]. When f_1 and $f_2 = \frac{1}{2}f_1$ are present, the map will read $x_{n+4} = x_n$ [Fig. 14.13(b)]. (These specific maps are overly simple compared to what one may encounter in a real flow, but they illustrate the idea.)

To reiterate, instead of describing the flow by the full solution $\mathbf{v}(\mathbf{x}, t)$ to the Navier Stokes equations and the flow's boundary conditions, we instead can construct the simple map $x_n \to x_{n+1}$ to characterize the flow. This procedure is known as a *Poincaré map.* The mountains have labored and brought forth a mouse! However, this mouse turns out to be all that we need. For the convection experiments, just the same period doubling behavior and approach to chaos is present in these maps as in the original phase-space diagram and in the full solution to the fluid dynamical equations; and when observed in the Poincaré maps, it looks qualitatively the same as in the Feigenbaum sequence. It is remarkable that for a system with so many degrees of freedom, chaotic behavior can be observed by surpressing almost all of them.

If, in the period-doubling route to chaos, we compute the limiting ratio,

$$\mathcal{F} = \lim_{j\to\infty} \frac{a_j - a_{j-1}}{a_{j+1} - a_j}, \tag{14.22}$$

we find that it has the value 4.6692016090.... This (Feigenbaum) number seems to be a universal constant characteristic of most period doubling routes to chaos, independent of the particular map that was used. For example, if we had used

$$x_{n+1} = a \sin \pi x_n \tag{14.23}$$

we would have got the same constant.

The most famous illustration of the period doubling route to chaos is a classic experiment by Libchaber on convection in liquid helium. The temperature at a point was monitored with time as the temperature gradient was slowly increased. Initially, the temperature was found to oscillate with a single period, but then subharmonics start appearing one after another, until, eventually, the flow became turbulent. Libchaber was able to measure Feigenbaum's number accurate to about 3 per cent.

When chaos sets in, the evolution of the system becomes essentially incalculable. This is because, as can be shown mathematically, the future state, as measured by the values of a set of fluid variables at some subsequent time (or by the value of a map), becomes highly sensitive to the assumed initial conditions. Paths in phase space (or in the mapping) that start extremely close to one another diverge from each other exponentially rapidly with time.

This realisation, that many classical systems have an intrinsic unpredictability despite being deterministic from instant to instant, has been widely publicised in popularisations of research into chaos. However it is not particularly new. It was well understood, for example, by Poincaré at the turn of the century and watching the weather report on the nightly news bears witness to its dissemination into the popular culture! What *is* new and intriguing is the manner in which the transition from a deterministic to a non-predictable evolution happens.

Chaotic behavior is well documented in a variety of physical dynamical systems: electrical circuits, nonlinear pendula, dripping faucets and so on. The extent to which the principles that have been devised to describe chaos in these systems can also be applied to general fluid turbulence remains a matter for debate. There is no question that there are similarities and there has been quantitative success in applying chaos results to a limited form of turbulent convection. However, most forms of turbulence are not so easily described and there is still a huge gap between these intriguing analyses and practical application to natural and technological flows.

****

EXERCISES

Exercise 14.9 *Problem: Feigenbaum Sequence*
Use a computer (or pocket calculator) to calculate the first five critical parameters a_j in the Feigenbaum sequence, Eq. (14.21). Hence verify that the ratio of successive differences, tends toward the limit quoted in Eq. (14.22). (Hint. You might find it helpful to construct a graph to find suitable starting values, x_1 and starting parameters a.)

Exercise 14.10 *Example: Lyapunov Exponent*
Consider the logistic Eq. (14.21) for the special case $a = 1$, which is large enough to ensure that chaos has set in.

(i) Make the substitution $x_n = \sin^2 \pi\theta_n$ and show that the equation can be expressed in the form $\theta_{n+1} = 2\theta_n(\mathrm{mod} 1)$.

(ii) Hence write θ_n as a "binimal" (binary decimal), e.g. 0.1011100101001. Explain what happens to this number in each successive iteration.

(iii) Now suppose that an error is made in the i'th digit of the starting binimal. When will it cause a major error in the predicted value of x_n?

(iv) If the error after n iterations is written ϵ_n, show that the Lyapunov exponent p defined by
$$p = \lim_{n\to\infty} \frac{1}{n} \ln \left| \frac{\epsilon_n}{\epsilon_0} \right|$$
is $\ln 2$. Lyapunov exponents play an important role in the theory of dynamical systems.

Exercise 14.11 *Example: Strange Attractors*
Another interesting one-dimensional map is provided by the recursion relation,
$$x_{n+1} = a(1 - 2|x_n - \frac{1}{2}|)$$

(i) Consider the asymptotic behavior of the variable x_n for different values of the parameter a both parameters being confined to the interval $[0, 1]$. In particular find that for $0 < a < a_{crit}$, the sequence x_n converges to a stable fixed point. However, for $a_{crit} < a < 1$, the sequence wanders chaotically through some interval $[x_{min}, x_{max}]$.

(ii) Using a pocket calculator or a computer, calculate the value of a_{crit} and the interval $[x_{min}, x_{max}]$ for $a = 0.8$.

(iii) The interval $[x_{min}, x_{max}]$ is an example of a *strange attractor*. It has the property that if we consider sequences with arbitrary close starting values, they will eventually diverge. Show that the attractor is strange by computing the sequences with $a = 0.8$ and starting values $x_1 = 0.5, 0.51, 0.501, 0.5001$. Determine the number of iterations n_ϵ required to produce significiant divergence as a function of $\epsilon = x_1 - 0.5$. It is claimed that $n_\epsilon \sim -\ln_2(\epsilon)$. Can you verify this? Note that the onset of chaos was quite sudden in this case unlike the behavior exhibited by the Feigenbaum sequence.

Exercise 14.12 *Problem: Lorenz equations*
One of the first discoveries of chaos in a mathematical model was by Lorenz, who made a simple model of atmospheric convection. In this model, the temperature and velocity field are characterized by three variables, x, y, z, which satisfy the coupled, nonlinear differential equations.
$$\begin{aligned}\dot{x} &= 10(y - x)\\ \dot{y} &= -xz + 28x - y\\ \dot{z} &= xy - 8z/3\end{aligned}$$
(The precise definitions of x, y, z need not concern us here.) Integrate these equations numerically to show that x, y, z follow non-repeating orbits in the three dimensional phase space that they span, but follow certain broadly defined paths in this space. (It may be helpful to plot out the trajectories of pairs of the dependent variables.)

****

Bibliography

Adair, R. K. 1990. *The Physics of Baseball*, New York: Harper and Row.

Drazin, P. G. and Reid, W. H. 1981. *Hydrodynamic Stability*, Cambridge: Cambridge University Press.

Lighthill, M. J. 1986. *An Informal Introduction to Theoretical Fluid Mechanics*, Oxford: Oxford Science Publications.

Feigenbaum, M. 1978. "Universal behavior in nonlinear systems," *J. Stat. Phys.*, **19**, 25.

Landau, L. D. and Lifshitz, E. M. 1959. *Fluid Mechanics*, Reading, Massachusetts: Addison Wesley.

Ott, E. 1982. "Strange attractors and chaotic motions of dynamical systems" *Rev. Mod. Phys.*, **53**, 655.

Ott, E. 1993. *Chaos in Dynamical Systems*, Cambridge: Cambridge University press.

Sagdeev, R. Z., Usikov, D. A., and Zaslovsky, G. M. 1988. *Non-Linear Physics from the Pendulum to Turbulence and Chaos*, Harwood.

Tennekes, H. and Lumley, J. L. 1972. *A First Course on Turbulence*, Cambridge: MIT Press.

Tritton, D. J. 1977. *Physical Fluid Dynamics*, New York: Van Nostrand Reinhold.

Van Dyke, M. 1982. *An Album of Fluid Flow*, Stanford: Parabolic Press.